# Depth profiles of defects in C-ion-irradiated steel determined by a least-squares fit of $S$ parameters from variable-energy positron annihilation

Takeo Aruga and Saburo Takamura
*Tokai Research Establishment, Japan Atomic Energy Research Institute, Tokai-mura, Naka-gun, Ibaraki-ken 319-11, Japan*

Masahumi Hirose and Yasuo Itoh
*Research Center for Nuclear Science and Technology, The University of Tokyo, Tokai-mura, Naka-gun, Ibaraki-ken 319-11, Japan*
(Received 9 June 1992)

A method for reconstructing the depth profile of defects in ion-irradiated samples with use of slow positrons is presented. The depth profiles of vacancy-type defects in the 316 stainless-steel sample irradiated with 250-keV carbon ions to a dose of $9.2\times10^{18}/m^2$ at room temperature has been calculated from Doppler-broadening $S$ parameters measured as a function of the positron energy. Without assuming any specific shape for the defect profiles, the defect profiling is made by a least-squares fitting method. The resulting profile shows that the defect distribution peaks at a depth smaller than that for the predicted damage peak, suggesting that the implanted carbon atoms enhance the defect annihilation by recombinations.

## I. INTRODUCTION

Since the studies of Triftshäuser and Kögel,[1-3] variable-energy positron-beam techniques have been applied to depth profiling of defects introduced in metal samples by ion irradiations,[4-7] as well as to semiconductor studies in depth profiling defects either associated with molecular-beam epitaxially-grown silicon epilayers,[8] or induced in crystalline silicon by ion implantation.[9,10] The principle utilized in these works stems from the observation by MacKenzie[11,12] that one could distinguish between annihilation line shapes in different metals and measure quantitatively the influence of lattice defects introduced by plastic deformation or by heating.

The fundamental principles of utilizing variable-energy slow-positron beams in defect profiling have been reviewed in detail by Schultz and Lynn.[13] The Doppler broadening of the $\gamma$-ray spectrum is determined by the momentum distribution of the $e^+$-$e^-$ system prior to annihilation. The spectrum resulting from positrons diffusing within a perfect lattice and annihilating with both conduction and core electrons has a more broadened spectrum around the annihilation peak at 511 keV, as compared with the spectrum from trapped positrons, due to a significant annihilation with more energetic core electrons. In a sample containing open-volume defects, such as vacancies, the probability for positrons to be trapped in these sites is enhanced and the total electron density as well as the core-electron fraction there are reduced. This results in a reduction in the Doppler broadening or in a narrowing of the annihilation peak. Several studies have been made to extract information on the defect depth profiles in the near-surface region in ion-implanted samples from changes in the Doppler-broadening line-shape $S$ parameters measured as a function of the positron energy. These procedures have assumed either a Gaussian profile[6] or box-shaped, i.e., truncated flat, profile[5,9] for the defect in fitting process for the observed $S$ parameter.

In the present study, the defect profiling is made by use of a least-squares fitting method, without resorting to any specific shape for the defect profile in a 316 stainless-steel sample irradiated with 250-keV carbon ions.

## II. EXPERIMENT

The 316 stainless-steel sample used in this study was solution annealed for 0.5 h at 1323 K in a vacuum after cold rolling to 0.2 mm thick and being shaped, to a size of $20\times20$ mm$^2$ and then abrasive and finally electrochemical polishing. The chemical composition was analyzed to be Fe-0.058C-0.61Si-1.80Mn-0.028P-0.003S-13.52Ni-16.75Cr-2.46Mo-0.005Ti-0.01Nb-0.004N in mass percent. The whole area of the sample was irradiated with a defocused 250-keV C-ion beam at room temperature with an ion flux of $3.9\times10^{15}/m^2s$ to a dose of $9.2\times10^{18}/m^2$ by using a Van de Graaff accelerator at Japan Atomic Energy Research Institute (JAERI). The irradiation is predicted to produce a peak displacement damage of 0.15 DPA (displacements per atom) around the depths of 250–270 nm and inject carbon atoms to about 500 at. ppm there, by TRIM85 computer code[14] calculation, as shown in Fig. 1.

The $S$-parameter measurements were conducted by using an apparatus illustrated in Fig. 2, which was composed of a $^{22}$Na positron source with an intensity of $1.5\times10^8$ Bq; a single-crystal W(100) foil of 1 $\mu$m thickness which was annealed in an UHV chamber at 2273 K to remove defects and was attached closely to the source for moderating positrons; a tungsten mesh placed in front of the moderator to extract and accelerate the emitted positrons to 15 eV; solenoid coils supplying a magnetic filed of 60–80 gauss for bending the beam to eliminate high-energy-positron background; an accelerating system supplying 0–8 kV above the ground potential between accelerating terminal flanges placed between focusing Helmholtz coils and 0 to $-8$ kV between the specimen and the ground. A high-purity germanium detector of

 

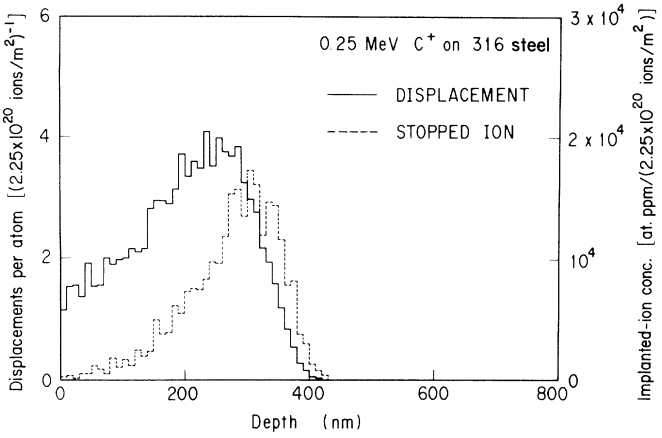


FIG. 1. Depth profiles of displacement damage and stopped ions in 316 stainless steel irradiated with 250-keV C ions to a dose of $2.25\times10^{20}$ ions/m$^2$, or (10 mA/m$^2$)$\times$1h irradiation.

energy resolution capability of 1.1 keV at 511 keV is used with a multichannel energy analyzing system for measuring annihilation $\gamma$ spectra. The beam profile was monitored by microchannel plate assembly with a phosphorescent plate. The diameter of the beam spot at the sample position was about 3 mm with a typical beam intensity of $3\times10^4$/s.

The $S$ parameters of annihilation-radiation spectra around 511 keV for monoenergetic positrons incident on the sample were obtained as a ratio of the counts in 11 channels corresponding to 3.6 (i.e., $\pm1.8$) keV around the peak to the total counts in 80 channels corresponding to 35 ($\pm17.5$) keV around the peak. The parameters were measured as a function of positron energies from 15 eV–16 keV at maximum. The positron with energy of 16 keV is predicted to have an average stopping range as deep as 420 nm, which is larger by 1.5 times than the projected range of 250-keV C ions in the sample. Therefore, the present measurements are considered to cover all well depths where the irradiation-induced defects may exist. The measurements were made before and after the irradiation, and also after isochronal anneals for 0.5 h up to the highest temperature of 823 K. The total count around

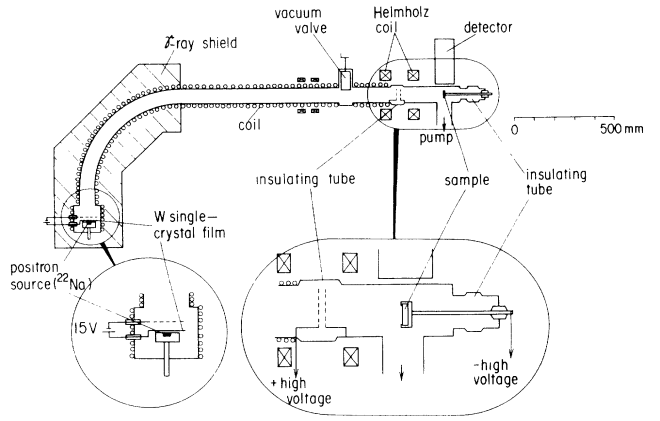


FIG. 2. Schematic experimental setup of the slow-positron system for positron energies up to 16 keV (see text for details).

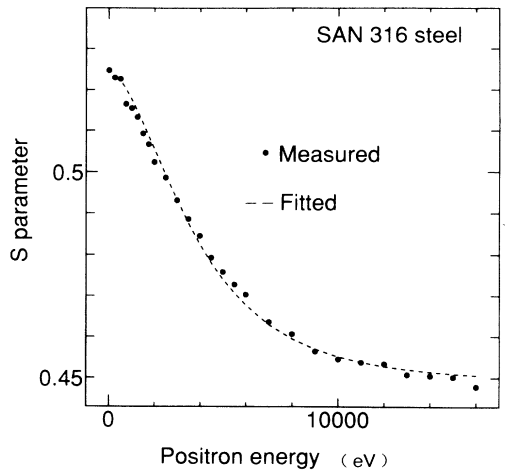


FIG. 3. Doppler-broadening $S$ parameters as a function of the incident-positron energy for unirradiated, solution-annealed (SAN) 316 stainless steel. Dashed curve shows the least-squares fit for the $S$ parameters.

the peak for each energy of positron was accumulated to $(4.9-5.3)\times10^5$ in 1800 s.

## III. EXPERIMENTAL RESULTS

Figure 3 shows the positron-energy dependence of the $S$ parameters measured for the solution-annealed 316 stainless-steel sample and a fitted curve of the $S$ parameter obtained as described below. The $S$ parameter decreases monotonically with increasing positron energy and shows a saturation tendency above 10 keV for the annealed sample. However, the complete independence of the $S$ parameter on the positron energy has not been obtained for the present highest positron energy of 16 keV. Figure 4 shows the positron-energy dependencies of the $S$ parameters for the sample after irradiation with 250-keV

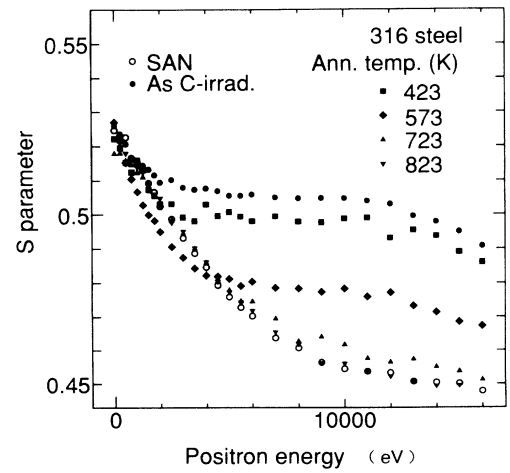


FIG. 4. Positron-energy dependencies of the $S$ parameters measured for the 316 stainless-steel sample after 250-keV C-ion irradiation to a dose of $9.2\times10^{18}$/m$^2$ and those measured after isochronal anneals at temperatures shown after the irradiation, along with the data measured for the solution-annealed (SAN) sample before irradiation.

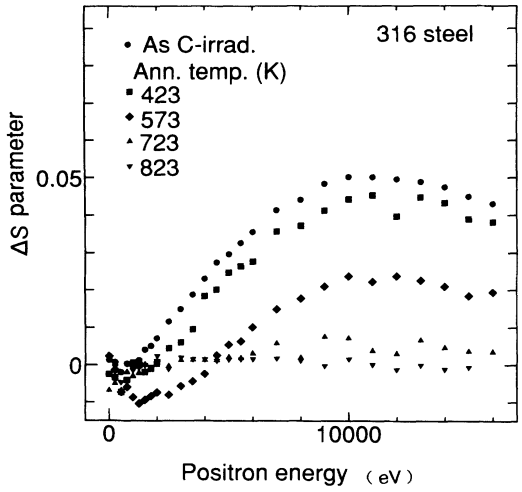


FIG. 5. $\Delta S$, i.e., difference of $S$ parameters from the values measured for the unirradiated, solution-annealed (SAN) sample.

C ions to $9.2\times10^{18}$ m$^2$ and after annealing for 0.5 h at 423, 573, 723, and 823 K along with the data of the unirradiated sample for comparison. The $S$ parameter increases after the C-ion irradiation for positron energies above 2 keV and the increase over those before the irradiation peaks at about 10 keV, which is easily seen in Fig. 5, where the differences of the $S$ parameter between those after the irradiation and before irradiation, or $\Delta S$ parameters, are plotted. Since the average stopping range of 10-keV positrons is about 200 nm in steel, as described below, the vacancy-type defects seem to peak at smaller depths than the peak of ion-radiation damages.

From the decrease of the $S$ parameter after the anneal at 573 K as compared with those after the irradiation, the remarkable recovery of the defects is revealed to take place after the anneal. It is seen that defects produced by the C-ion irradiation almost completely anneal out after the anneal at 823 K, since the $S$ parameters after the 823-K anneal agree with those before the irradiation. It is noted that the $S$ parameters after the irradiation have large deviations from those before the irradiation even for the highest positron energy of 16 keV, which implies that radiation-produced defects would exist far beyond the ion range of 250–270 nm. Presumably this may occur through atomic displacements by sequential atom collisions and by vacancy diffusion along the steep gradient of the distribution of radiation-produced defects (Fig. 1).

## IV. ANALYSIS

According to the model for $S$-parameter analyses developed and described in detail by Lynn and collaborators,[5,13] the observed $S$ parameter $S(E)$ for positrons of energy $E$ can be expressed by using the fraction $F(E)$ of positrons annihilating at the surface, in the bulk and in the defect and the characteristic Doppler-broadened line-shape parameter $S$ for a positron annihilating at the surface, in the bulk or in the defect:

$$S(E)=F_s(E)S_s+F_b(E)S_b+F_d(E)S_d \ , \tag{1}$$

where the subscripts represent the positron-annihilation site at the surface, in the bulk, and in the defect. The theoretical expressions for $F_s$, $F_b$, and $F_d$ are related to the positron motion described through the steady-state, one-dimensional diffusion equation:

$$D\nabla^2 n(x,E)-[\lambda_b+\mu C(x)]n(x,E)+P(x,E)=0 \ , \tag{2}$$

where $D$ is the positron diffusion coefficient, $n(x,E)$ is the positron density at the depth $x$ for the incident positron energy $E$, $C(x)$ is the defect density at depth $x$, $\lambda_b$ is the annihilation rate in the bulk, $\mu$ is the specific trapping rate for the defect, and $P(x,E)$ is the stopping-range distribution or the implantation profile for incident-positron energy $E$. It has been shown that $P(x,E)$ has the following form:[15]

$$P(x,E)=\frac{mx^{m-1}}{x_0^m}\exp[-(x/x_0)^m] \ . \tag{3}$$

The parameter $m$ has been found to be about 1.9 and $x_0$ can be expressed as $x_0=\alpha E^n/\rho$, where $\rho$ is the material density in g/cm$^3$, $E$ in keV, $\alpha=4.5$ $\mu$g/cm$^2$, and $n=1.6$. Figure 6 shows the estimated positron-stopping profiles in the steel ($\rho=8$ g/cm$^3$) for the positron energies from 6

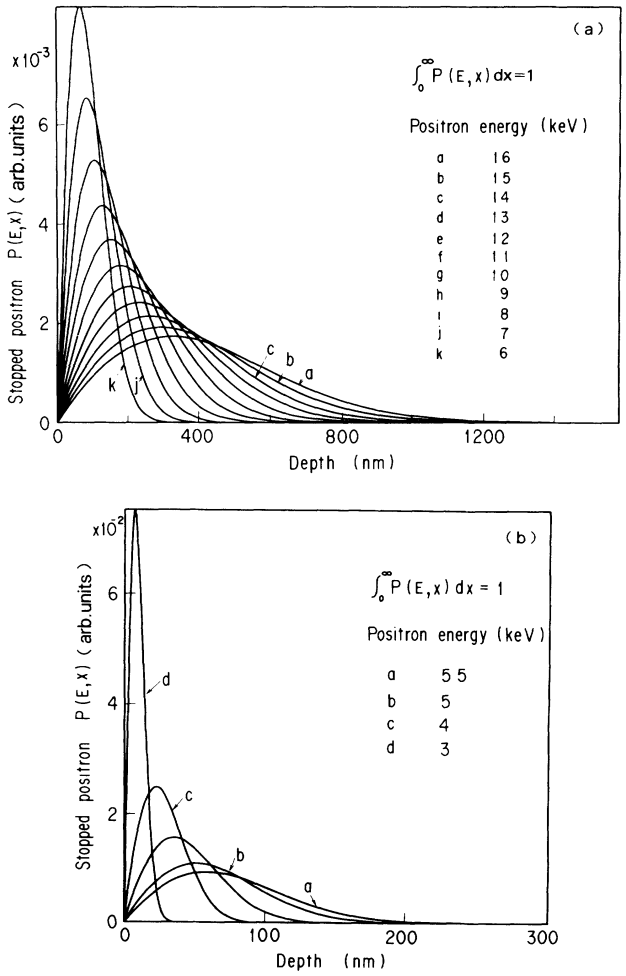


FIG. 6. Depth profiles of stopped positrons of energies (a) from 6 to 16 keV and (b) 3 to 5.5 keV, incident on 316 stainless steel.

to 16 keV and 3 to 5.5 keV. The relative fractions $F_s$, $F_b$, and $F_d$ are calculated as follows:

$$F_s(E) = -D\nabla n(x,E)|_{x=0} , \quad (4)$$

$$F_b(E) = \int_0^\infty \lambda_b n(x,E)dx , \quad (5)$$

$$F_d(E) = \int_0^\infty \mu C(x) n(x,E)dx . \quad (6)$$

Since the positron-implantation profile is normalized to 1.0, i.e., $\int_0^\infty P(x,E)dx = 1.0$, the following relation holds:

$$F_s(E) + F_b(E) + F_d(E) = 1 , \quad (7)$$

which is obtained by integration of Eq. (2). For the solution-annealed sample, defect density can be assumed to be zero, then, the positron density $n_0(x,E)$ satisfies

$$D\nabla^2 n_0(x,E) - \lambda_b n_0(x,E) + P(x,E) = 0 . \quad (8)$$

The integration of Eq. (8) leads to

$$F_{s0}(E) + F_{b0}(E) = 1 , \quad (9)$$

and, for the observed $S$ parameter $S_0(E)$,

$$S_0(E) = F_{s0}(E)S_s + F_{b0}(E)S_b , \quad (10)$$

where the subscript 0 means an unirradiated sample or a defect-free one. A more accurate expression for detecting the defect as a function of energy and, therefore, for profiling the defect is

$$\Delta S(E) = S(E) - S_0(E) = \Delta F_s(E)(S_s - S_b) + F_d(E)(S_d - S_b) , \quad (11)$$

where $\Delta F_s(E)$, given by

$$\Delta F_s(E) = F_s(E) - F_{s0}(E) , \quad (12)$$

is the difference of the fraction of positrons annihilating at the surface after the irradiation from that before irradiation for the same sample. $\Delta S(E)$ for the present measurement is already shown in Fig. 5.

We obtain the basic equation to calculate the defect depth profile after inserting Eq. (6) into (11), namely,

$$\Delta S(E) - \Delta F_s(E)(S_s - S_b) = (S_d - S_b)\int_0^\infty \mu C(x) n(x,E)dx . \quad (13)$$

We can find the best-fit solution for $C(x)$, which satisfies both Eqs. (13) and (2) by iteration.

We use 1 $cm^2/s$ for $D$, the diffusion constant for thermalized positrons in the steel, which is assumed not to differ so much from that in nickel[5] or in iron.[13] Besides, the trapping and annihilation behavior of positrons for vacancies in an austenitic steel seems not to differ, so long as an average lifetime is compared, from that in nickel and iron:[16] 178 ps in electron-irradiated steel, 170 ps in iron, and 180 ps in cold-worked nickel. On the other hand, $\lambda_b$ is so calculated that $L_0 = \sqrt{D/\lambda_b}$ and $S_b$ can give the best-fit curve to the observed $S(E)$ for the unirradiated sample, as shown in Fig. 3; $L_0 = 51.5$ nm, therefore, $\lambda_b = D/L_0^2 = 3.8\times10^{10}/s$ and $S_b = 0.448$ are fixed. In the fitting process to find $L_0$ and $S_b$, the relation

$$F_{s0}(E) = -D\nabla n_0(x,E)|_{x=0} = \int_0^\infty P(x,E)\exp(-x/L_0)dx , \quad (14)$$

and Eqs. (9) and (10) have been used. For $S_s$, the observed $S$ parameter for $E = 15$ eV, i.e., a value of 0.5247, was adopted. The value of $S_b$, 0.448, obtained by fitting is in reasonable agreement with the observed $S$ parameters above 10 keV.

The expression of Eq. (13) in the difference form gives

$$Y_i = \sum_{J=1}^{J_{max}} n_{iJ}X_J \quad (i = 1,2,\ldots,I) , \quad (15)$$

where $Y_i$, $n_{iJ}$, and $X_J$ are defined as

$$Y_i = \frac{\Delta S(E_i) - \Delta F_s(E_i)(S_s - S_b)}{S_d - S_b} , \quad (16)$$

$$n_{iJ} = \sum_{j\in J} n(x_j,E_i)\Delta x_j , \quad (17)$$

$$X_J = \mu\overline{C(x_J)} . \quad (18)$$

Subscripts $i$ $(=1,2,\ldots,I)$ mean the incident-positron energies and $j,J$ the mesh number for depths: $j$ for a finer mesh of 0.2–2 nm width, which is used in solving the positron diffusion equations (2) and (8), and $J$ $(=1,2,\ldots,J_{max})$ for a coarse mesh of 50 nm, over which $\mu C(x)$ is assumed to be averaged to $X_J = \mu\overline{C(x_J)}$ and is expressed as $\mu C_J$ for brevity. Equation (15) is the linear equation for $J_{max}$ unknowns of $X_J$, where $J_{max}$ is 60, for a example, when the $J$-mesh width is taken as 50 nm to cover the maximum depth of 3000 nm. On the other hand, the number of equations $I$ is the number of incident-positron energies, 27. Therefore, the unique and exact solution cannot be obtained. However, the well-known least-squares method[17] gives the best-fit solution for $\mu C_J$.

Rewriting Eq. (15) using a vector and matrix notation,

$$\underline{N}\mathbf{X} = \mathbf{Y} , \quad (19)$$

where elements of the matrix $\underline{N}$ are $n_{iJ}$. The problem to find the best-fit solution of $X_J$ $(=\mu C_J)$ is replaced by the problem to minimize $|\mathbf{X}|$ under the constraint of $\underline{N}\mathbf{X} = \mathbf{Y}$. Using a Lagrange multiplier vector $\mathbf{W}$, let $L$ be

$$L = |\mathbf{X}| + 2\mathbf{W}^T(\mathbf{Y} - \underline{N}\mathbf{X}) = \mathbf{X}^T\mathbf{X} + 2\mathbf{W}^T(\mathbf{Y} - \underline{N}\mathbf{X}) . \quad (20)$$

Then the total differential of $L$ with respect to $d\mathbf{X}$ must vanish, i.e.,

$$dL = 2\mathbf{X}^T d\mathbf{X} - 2\mathbf{W}^T\underline{N}\,d\mathbf{X} = 2(\mathbf{X}^T - \mathbf{W}^T\underline{N})d\mathbf{X} = 0 , \quad (21)$$

which is satisfied by

$$\mathbf{X}^T = \mathbf{W}^T\underline{N} . \quad (22)$$

Transposing both sides of Eq. (22), and inserting $\mathbf{X} = \underline{N}^T\mathbf{W}$ into Eq. (19), we obtain $\underline{N}\underline{N}^T\mathbf{W} = \mathbf{Y}$ and finally we have

$$\mathbf{X}=\underline{N}^T(\underline{N}\underline{N}^T)^{-1}\mathbf{Y} . \quad (23)$$

Since the matrix $\underline{N}\underline{N}^T$ is positive, definite, and nonsingular, the best-fit solution of $X_J=\mu C_J$ can be obtained.

In general, both $n(x,E)$ and $\mu C_J(x)$ cannot be known simultaneously. Therefore, an iterative process must be applied to find the best fit $\mu C_J(x)$ or $X_J$ ($J=1,2,\ldots,J_{\max}$) as the solution of Eq. (23). In the first step of the iteration, $\underline{N}_0$ is taken as the initial guess, where $\underline{N}_0$ is the matrix obtained as the solution of Eq. (8), the positron diffusion equation in the defect-free sample. The boundary conditions for Eq. (8) and for Eq. (2) as well, are $n(0,E)=0$ and $n(\infty,E)=0$, where $x=3000$ nm is taken as $x=\infty$ for the highest positron energy of 16 keV, since the profiles of $n(x,E)$ do not vary if a depth larger than 3000 nm is taken as $x=\infty$. Then, the best-fit solution for the first iteration, $\mathbf{X}^{(1)}$, is given by Eq. (23), letting $\underline{N}=\underline{N}_0$ and by using the measured $\Delta S(E_i)$ and the current $\Delta F_s(E_i)$ and $S_d$ in Eq. (16). For the next iteration, $X^{(1)}$ is put into Eq. (2), the solution of which is no longer equal to $\underline{N}_0$, since the defect profile term, $\mathbf{X}^{(1)}=\mu\mathbf{C}(x)$, as obtained above, is included in the positron diffusion equation (2). The iterative process is repeated until the value of $S_d$ obtained by the following least-squares fit for each step converges to the preassigned target value $S_d^t$:

$$S_d=\frac{\sum_{i=1}^{I}F_d(E_i)[\Delta S(E_i)-\Delta F_s(E_i)(S_s-S_b)]}{\sum_{i=1}^{I}[F_d(E_i)]^2}+S_b . \quad (24)$$

For $F_d(E_i)$ and $F_s(E_i)$ in the equation above, $\mu\mathbf{C}(x)$ and $n(x,E)$ obtained after the current iteration step are used in Eqs. (4), (6), and (12), and it is assumed that both $D$ and $\lambda_b$ are unchanged by the presence of defects. Although the experimentally determined value for $S_d$ is desired, it is assumed that $S_d$ is 15% larger than the experimentally fitted $S_b$, i.e., $S_d=0.515$. This value is used for the first step of Eq. (15) or in Eq. (16) as the initial guess and the target value for $S_d$.

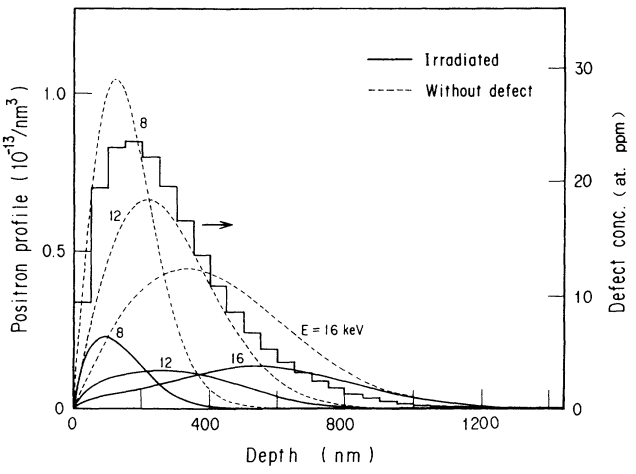


FIG. 7. Depth profiles of diffused positrons after being thermalized for incident energies of 8, 12, and 16 keV: dashed curves for unirradiated, defect-free 316 steel sample, solid curves for the irradiated sample as the convergent solution of iterative procedures. Solid staircase shows the convergent solution of the defect profile for the sample after 250-keV C-ion irradiation.

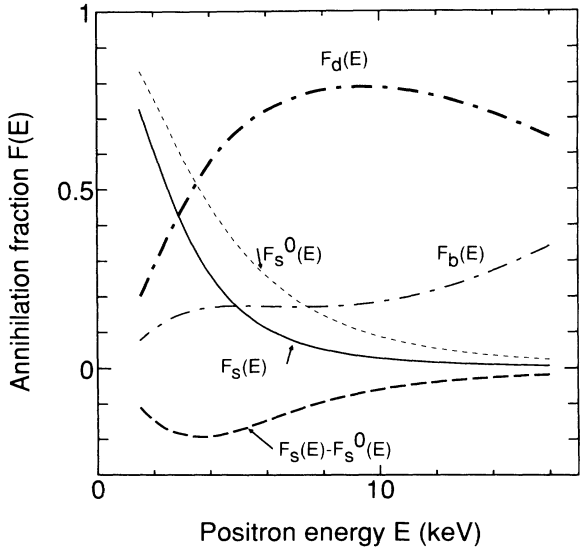


FIG. 8. Relative annihilation fractions as a function of the incident positron energies for the 316 steel sample after the irradiation, which are obtained after convergence in iterative procedures. $F_s^0$ or $F_s(E)$ before the irradiation is shown for a comparison.

In the Figures from 7 to 11, the calculational results for reconstructing the defect profiles after convergence in the iterative procedures are shown. In Fig. 7, dashed curves show the positron profiles for three representative energies of positrons incident on the defect-free sample, which are obtained as solutions of Eq. (8) by using respective positron implantation depth profiles shown in Fig. 6(a). Solid curves show the respective positron depth profiles in the irradiated sample, which are obtained as solutions of Eq. (2), which is including the term for a

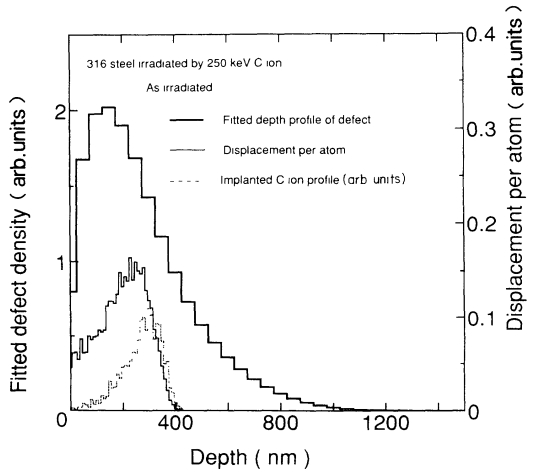


FIG. 9. Fitted defect density profile in 316 steel irradiated with 250-keV C ions, compared with the TRIM-code prediction.

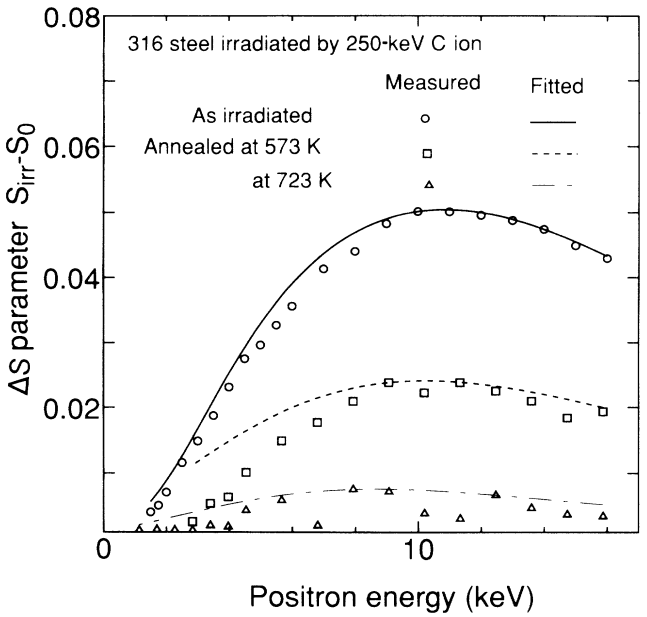


FIG. 10. Comparisons between measured and fitted $\Delta S$ parameter after convergence of iterative procedures for the 316 steel sample after the irradiation and the anneals for 0.5 h at 573 and 723 K.

depth profile of the defects $\mu C(x)$, where $\mu C_J$ is obtained as a solution of Eq. (15) and is shown as a staircase in the figure, for the as-irradiated sample. The relative annihilation fractions $F_s(E)$, $F_b(E)$, and $F_d(E)$ for the as-irradiated sample after the convergence along with $F_{s0}(E)$ in the defect-free sample are shown in Fig. 8 as a function of the positron energy.

Figure 9 compares the fitted defect depth profile in the as-irradiated sample with the displacement-damage depth profile obtained by the TRIM code. Whereas the damage

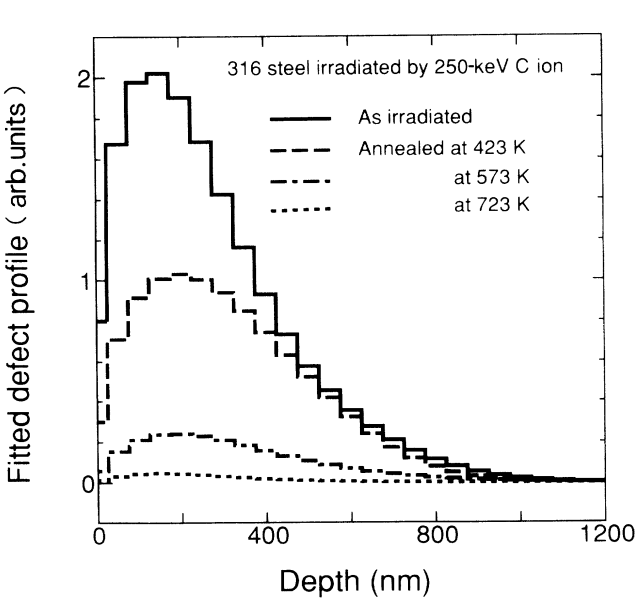


FIG. 11. Fitted defect profiles obtained after convergence of iterative procedures for the 316 steel sample after the irradiation and the anneals for 0.5 h at 423, 573, and 723 K.

depth profile produced by 250-keV C-ion irradiation is predicted to be distributed up to a depth of 400 nm and to peak at depths of about 250–270 nm, the defect depth profile obtained by $S$-parameter fitting extends up to over 800 nm, that is, deeper by twice than the TRIM-code prediction and peaks at a smaller depth from the surface than the prediction.

The fitted $\Delta S$-parameter curves are compared with the measured values in Fig. 10 for the as-irradiated sample and after anneals, and the corresponding fitted defect depth profiles are shown in Fig. 11. Note that the fitting is made for positron energies for which $\Delta S(E)$ shown in Fig. 5 is positive. Although the fitting is not satisfactory, especially for smaller $\Delta S(E)$ after the anneals and for lower positron energies, the defect depth profiles shown in Fig. 11 show the relative depth dependence of defect recovery quantitatively.

## V. DISCUSSION

The present analysis relies on a rather simple model for the diffusion and annihilation of positrons in steel. Other factors which should have been taken into account in a more fully developed model include the following:[5] the influence of epithermal-positron annihilation on the $S$ parameters, which should be substantial for high defect concentrations; possible saturation behavior in the relative annihilation fraction $F_d(E)$, which is a function of the defect concentration; and the dependence of the characteristic $S$ parameter for defects, $S_d$, on the defect type, such as single vacancy, clustered vacancy, dislocation loop, and so on. However, few experimental measurements have been made concerning these factors, especially for alloys such as 316 stainless steel. Therefore, the presently adopted or assumed values are expected to deviate somewhat from the exact ones: the values of the positron diffusion coefficient $D$, which is assumed to be 1 $cm^2/s$, the specific trapping rate for the defect $\mu = 10^{14}/s$, and characteristic $S$ parameter for the defect $S_d = 0.515$. Consequently, the presently reconstructed depth profiles of defects can be varied to an extent by which the adopted values for $D$, $S_d$, and $\mu$ are varied. For example, if we use a value larger, say, by 10% than the present one for $D$, keeping the positron diffusion length $L_0 = \sqrt{D/\lambda_b}$ obtained by fitting to the measured $S$ parameters unchanged, the positron depth profiles after diffusion are distributed with slightly lowered values and with a slightly larger spread, the resultant defect depth profiles are calculated to be slightly larger. An assumption of smaller value for target $S_d^t$, a preassigned characteristic $S$ parameter for the defect, results in the larger values for defect depth profiles, although in the small change in the shape.

Presently, the value of $1.15S_b$ is assumed for $S_d$. It is reported for silicon that $S_d$ of vacancy defect is $1.034S_b$ as measured from saturation positron trapping,[9] while $S_d$ of $1.18S_b$ is reported for He-implanted pure nickel as obtained by fitting the defect depth profile to observed $\Delta S$, although under the assumption of a truncated, flat depth profile for the defect.[5] Thus, the ratio of $S_d$ to $S_b$ can vary vastly depending on the material's being semiconductor or metal. However, since it seems plausible to as-

sume that trapping and annihilation behavior of positrons in the steel may not differ much from those in pure nickel, as described in the previous section, the ratio of 1.15 is adopted for the present analysis. Besides, the value of $S_d$, 0.515, corresponds to $0.98S_s$ in the present study, which is close to $0.97S_s$ for pure nickel in the case cited above, where each $S_s$ has been obtained by fitting the measured $S$ for the defect-free sample. Meanwhile, the value of $S_d^i$ can be estimated experimentally, as described in Ref. 9, by measuring the $S$-parameter changes for a fixed positron energy about 10 keV for 250-keV C-ion irradiation sequentially as a function of the irradiation dose for the same sample in which a controlled quantity of defects is introduced by irradiations and by fitting the $S$-parameter changes. Nevertheless, the present depth profiles of defects obtained by the least-squares fit to the measured $S$-parameter values are considered representative of the depth profiles of defects which would be realized in the sample, since no specific defect depth profiles are assumed provisionally, such as the Gaussian or truncated uniform distribution.

If positrons with energies higher than 16 keV were used in $S$-parameter measurements, the fitted defect concentration would be raised slightly at depths larger than a certain depth, 800 nm, for example. However, the basic shape of the defect depth profile is not expected to change, because a fairly large fraction of positrons with 16 keV incident on the sample is distributed far deeper than 800 nm and trapped by defects existing there (Fig. 7). The fitted defect depth profile in the as-irradiated sample reveals that the defects are distributed much greater depths than the damage simulation result and peak at smaller depths from the surface than the prediction. Like the injected self-interstitial atoms,[18] the carbon atoms implanted in the irradiation would enhance the recombination of radiation-produced defects and lower the defect concentration around the damage peak. Furthermore, the radiation-produced interstitial atoms are considered to have a larger change to migrate to the sample surface than vacancies to raise the vacancy concentration near the surface. As for the extended spreading of vacancy-type defects as deep as twice the predicted region of damage distribution, two possibilities are considered. First, at room-temperature irradiation, vacancies can diffuse along the steep gradient of the distribution of radiation-produced point defects into the region of larger depths, since it has been reported that vacancies migrate at 280 (Ref. 16) or 300 K (Ref. 19) and above in steel. Secondly, the nonlinear collisional effect seems to work in atomic displacements. Atomic collisions between moving atoms have been shown by simulation calculation[20] to transfer the energy of incident ions much deeper than the simple binary collisions between moving and stationary atoms.

Since the $S$-parameter increase due to single vacancies in nickel has been estimated to be about 6%,[21] the maximum change of about 10% in the present $S$ parameters measured after the irradiation as compared with that before irradiation (Fig. 4) suggests that positrons would be trapped by clustered vacancies. That the defects produced in the present irradiation and detected by positrons may be clustered vacancies is supported by the fact that these defects survive after the anneal at a high temperature of 723 K, as is shown in Fig. 4 or 5 in the difference between the $S$ parameter after 723 K anneal and before the C-ion irradiation, whereas the defects produced by 3-MeV electron irradiation in steel have been reported to disappear after an anneal for 0.5 h at 650 K.[16]

In the present analysis the fitted depth profile for defects is the total trapping rate, $\mu C(x)$, for thermalized positrons. Although the defects seem to be clustered vacancies, an average or most probable number of vacancies in the cluster cannot be defined merely from the $S$-parameter dependence on the positron energy. A joint measurement of positron lifetimes as a function of the positron energy together with that of $S$ parameters with use of a pulsed, variable-energy source[22] will provide information concerning the depth dependence for structures of the vacancy cluster. The maximum trapping rate for the as-irradiated sample that gives the peak in the defect depth profile is about 5.3 times larger than the bulk annihilation rate used, $\lambda_b$. If the value of the specific trapping rate, $\mu$ for the defect is known, one can evaluate the density of the defects, although without knowledge of the scale of the cluster. The defect concentration preliminarily shown in Fig. 7 is only converted from the fitted $\mu C_J$ by using an assumed value of $10^{14}$/s for $\mu$. The specific trapping rate for monovacancies in iron has been evaluated by a lifetime measurement to be about $1.1\times10^{15}$/s,[23] and the theoretical calculation has shown that, for small clusters, the trapping rate is scaled with the number of vacancies in the cluster.[24] The present use of $10^{14}$/s for $\mu$ is intended to give a 10-times-larger concentration for single vacancies, but still the fitted vacancy concentration at the peak corresponds to $1.7\times10^{-4}$ of the calculated displacement damage.

## VI. CONCLUSION

A calculational method for fitting the defect depth profile to the measured $S$ parameter from annihilation radiation of variable-energy positrons has been presented. Without resorting to any provisional shapes for the depth profile, the defect profiles in a 316 stainless-steel sample after irradiation with 250-keV C ions to a dose of $9.2\times10^{18}/m^2$ at room temperature and after anneals up to 823 K have been obtained. The radiation-produced defects are found to distribute twice deeper than the prediction by damage calculation and to peak at smaller depths than the prediction.

[1]W. Triftshäuser and G. Kögel, Phys. Rev. Lett. **48**, 1741 (1982).
[2]W. Triftshäuser and G. Kögel, J. Nucl. Mater. **111&112**, 687 (1982).
[3]W. Triftshäuser and G. Kögel, in *Positron Annihilation*, Proceedings of the Sixth International Conference on Positron Annihilation, Arlington, Texas, 1982, edited by P. G. Coleman *et al.* (North-Holland, Amsterdam, 1982), p. 142.
[4]S. Tanigawa, Y. Iwase, A. Uedono, and H. Sakairi, J. Nucl.

Mater. **133&134**, 463 (1985).
[5]K. G. Lynn, D. M. Chen, B. Nielsen, R. Pareja, and S. Myers, Phys. Rev. B **34**, 1449 (1986).
[6]A. Uedono, S. Tanigawa, and H. Sakairi, J. Nucl. Mater. **173**, 307 (1990).
[7]A. Uedono, S. Tanigawa, and H. Sakairi, J. Nucl. Mater. **184**, 191 (1991).
[8]P. J. Schultz, E. Tandberg, K. G. Lynn, B. Nielsen, T. E. Jackman, M. W. Denhoff, and G. C. Aers, Phys. Rev. Lett. **61**, 187 (1988).
[9]J. Keinonen, M. Hautala, E. Rauhala, L. Karttunen, A. Kuronen, J. Räisänen, J. Lahtinen, A. Vehanen, E. Punkka, and P. Hautojäarvi, Phys. Rev. B **37**, 8269 (1988).
[10]P. J. Simpson, M. Vos, I. V. Mitchell, C. Wu, and P. J. Schultz, Phys. Rev. B **44**, 12 180 (1991).
[11]I. K. MacKenzie, Phys. Lett. **30A**, 115 (1969).
[12]I. K. MacKenzie and P. C. Lichtenberger, Appl. Phys. **9**, 331 (1976).
[13]P. J. Shultz and K. G. Lynn, Rev. Mod. Phys. **60**, 701 (1988).
[14]J. F. Ziegler, J. P. Biersack, and U. Littmark, *The Stopping and Range of Ions in Solids* (Pergamon, New York, 1985), Vol. 1.
[15]S. Valkealahti and R. M. Nieminen, Appl. Phys. A **35**, 51 (1984).
[16]C. Corbel, C. Dimitrov, and P. Moser, in *Positron Annihilation* (Ref. 3), p. 535.
[17]S. Brandt, *Statistical and Computational Methods in Data Analysis* (North-Holland, Amsterdam, 1970), p. 176.
[18]D. B. Bullen, G. L. Kulcinski, and R. A. Dodd, Nucl. Instrum. Methods B **10/11**, 561 (1985).
[19]K. Nakata, S. Takamura, and I. Masaoka, J. Nucl. Mater. **131**, 53 (1985).
[20]Y. Yamamura, Nucl. Instrum. Methods B **33**, 493 (1988).
[21]L. C. Smedskjaer, M. J. Fluss, D. G. Legnini, M. K. Chason, and R. W. Siegel, J. Phys. F **11**, 2221 (1981).
[22]R. Suzuki, Y. Kobayashi, T. Mikado, H. Ohgaki, M. Chiwaki, T. Yamazaki, and T. Tomimasu, Jpn. J. Appl. Phys. **30**, L532 (1991).
[23]A. Vehanen, P. Hautojärvi, J. Johansson, and J. Yli-Kauppila, Phys. Rev. B **15**, 762 (1982).
[24]R. M. Nieminen and J. Laakkonen, Appl. Phys. **20**, 181 (1979).